(Received 22 June 2025, Accepted 3 August 2025, Scheduled 11 August 2025)

Wideband Circularly Polarized Dielectric Resonator Antenna Based on Double-Layer Metasurface

Wenhan Wan[1,2], Wusheng Ji[1,2,*], Zhaoyi Wang[1,2], and Xingyong Jiang[3]

[1] School of Electronic Engineering, Tianjin University of Technology and Education, Tianjin 300222, China
[2] Institute of Antenna and Microwave Techniques, Tianjin University of Technology and Education, Tianjin 300222, China
[3] Rofs Microsystem, Tianjin 300462, China

ABSTRACT: This paper presents a single-fed wideband circularly polarized high-gain dielectric resonator antenna (DRA) for KU-band applications. The proposed antenna consists of a cylindrical dielectric resonator on top, a double-layer metasurface structure in the middle, and a feeding substrate at the bottom. An asymmetric X-shaped slot coupling feed on the substrate enables circular polarization characteristic. The DRA incorporates a double-layer metasurface to broaden the 3 dB axial ratio bandwidth and enhance gain. Simulation results show that the antenna achieves a −10 dB impedance bandwidth of 24.2% (13.69–17.46 GHz), a 3 dB axial ratio bandwidth of 20.01% (14.05–17.2 GHz), with a peak gain of 9.89 dBi. The designed antenna operates in the KU-band and is suitable for wireless communication applications including satellite communications and global positioning systems.

1. INTRODUCTION

Dielectric resonator antenna (DRA) was first proposed by Long et al. in 1983 [1], followed by extensive research from scholars, yielding numerous achievements. DRAs possess excellent characteristics including low ohmic loss, high radiation efficiency, compact size, design flexibility, and wide operating bandwidth [2, 3], making them play a crucial role in modern wireless communication systems.

As the need for multimedia services and worldwide connectivity continues to rise, satellite systems have gained critical importance [4, 5]. The stringent requirements for dependable communication links and high-speed data transfer in satellite systems persistently propel the development of high-performance antennas. Polarization has been recognized as one of the most vital performance features when antennas are integrated with contemporary communication systems.

Circularly polarized antennas are prioritized over linearly polarized antennas in practical applications owing to their superior capabilities in minimizing polarization mismatch, alleviating multipath effects, and compensating for Faraday rotation [6, 7]. The realization of circular polarization (CP) currently employs two approaches: single-feed and dual-feed techniques [8]. While dual-feed techniques enable easier attainment of broader 3 dB axial ratio bandwidth than single-feed approaches, they necessitate intricate power dividers and hybrid coupling networks, leading to design complexity and bulky configurations, such as sequential tree-shaped arrays [9] and sequentially rotated dual-inline arrays [10].

Multiple approaches enable circular polarization through single-feed methods, such as employing customized dielectric resonator geometries, specialized feeding slots, multi-layer DRA configurations, and integration of metasurfaces or air-filled vias. In [11], a stepped-profile DRA excited by microstrip feed with hybrid split-ring/full-ring grounding realized 8.47% 3 dB axial ratio (AR) bandwidth and 7.6 dBi peak gain. Ref. [12] demonstrated circular polarization using a meandered microstrip feed, attaining 12.26% AR bandwidth albeit with 2.35 dBi gain. The S-profile stacked DRA configuration in [13] achieved 24.75% AR bandwidth while maintaining 7.32 dBi gain. A self-complementary metasurface design in [14] attained circular polarization through quasi-self-complementary properties, yielding 6.03 dBi gain. Circular air vias were employed in [15] to obtain 5.5% AR bandwidth with 7.1 dBi gain. Ref. [16] utilized dielectric via technology to achieve 26.7% AR bandwidth by considering perforated substrate as part of the DRA. Ref. [17] employed an inverted T-shaped slot structure for excitation, achieving approximately 10% AR bandwidth and 10.3 dBi gain. Ref. [18] utilized a cross-slot feed with a frequency selective surface superstrate, obtaining 2.97% AR bandwidth. Although the antennas in the aforementioned references all achieved circular polarization, none of these studies successfully established an optimal balance between axial ratio bandwidth and gain.

In recent studies, many scholars have utilized metasurfaces to improve antenna performance metrics [19]. With their polarization control characteristics, metasurfaces enable circular polarization and high gain when being placed above or beneath patches/radiators [20]. Typical implementations comprise metasurface-loaded slotted microstrip antennas [21] and layered asymmetric metasurfaces over rectangular patches [22]. Single-feed circularly polarized antennas can achieve enhanced axial ratio bandwidth and improved gain through metasurface integration while maintaining structural simplicity.

* Corresponding author: Wusheng Ji (jiwusheng@tute.edu.cn).

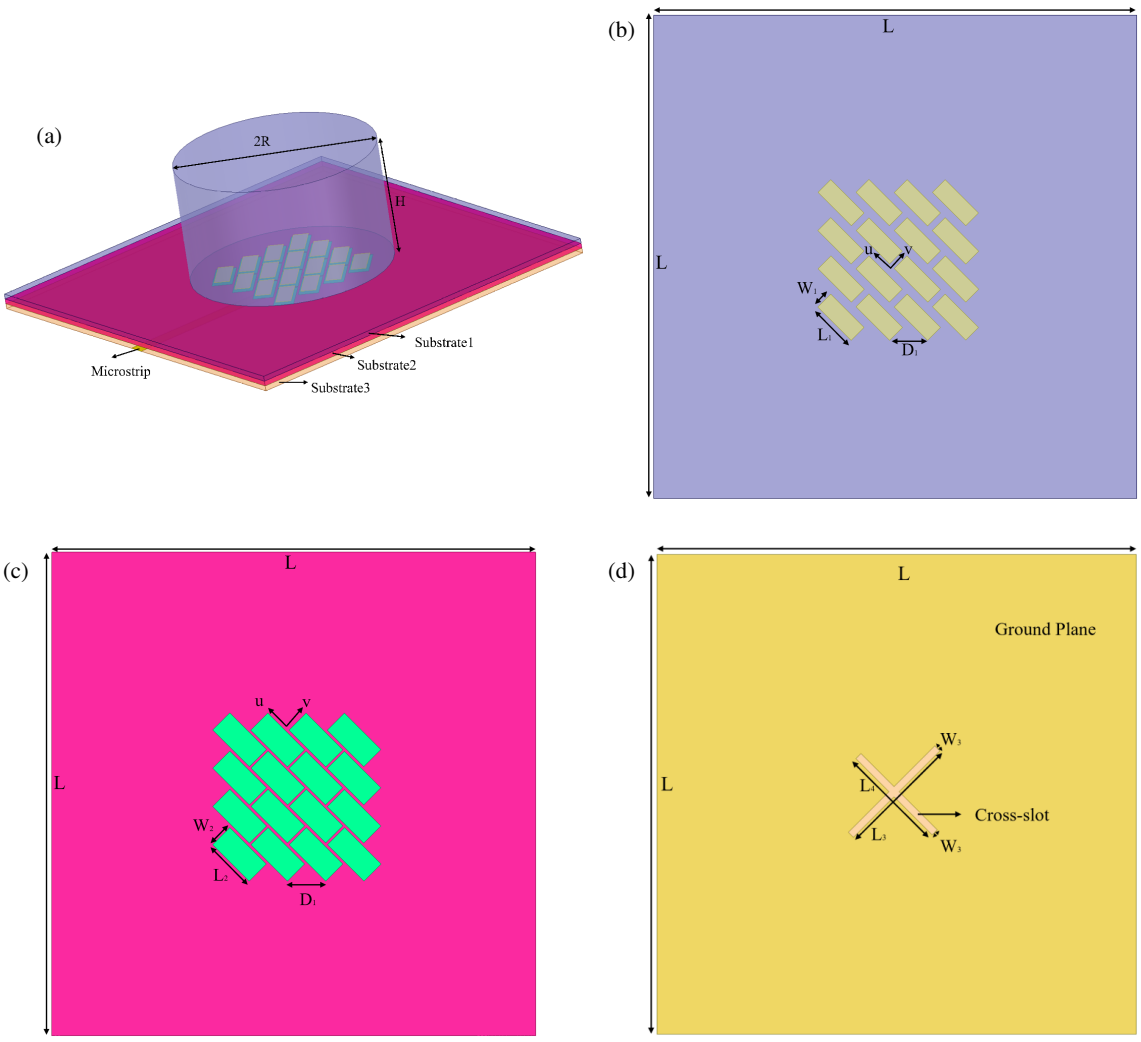

FIGURE 1. Configuration of the proposed antenna. (a) 3D view. (b) Top-layer metasurface. (c) Bottom-layer metasurface. (d) Top view of X-shaped groove.

In response to the gain deficiency in conventional single-feed CP antennas, we present a straightforward single-feed approach featuring asymmetric slot excitation integrated with a cylindrical DRA incorporating dual-layer metasurfaces, which realizes broadband circular polarization and enhanced gain performance. Electromagnetic simulations using High Frequency Structure Simulator (HFSS) software have demonstrated the antenna's superior characteristics.

2. ANTENNA DESIGN AND ANALYSIS

2.1. Antenna Structure

The proposed dielectric resonator antenna (DRA) shown in Figure 1 consists of three key components: a cylindrical dielectric resonator on top, a dual-layer metasurface structure in the middle, and a feeding substrate at the bottom. The top cylindrical DRA is fabricated from JJD07-1 dielectric ceramic material (relative permittivity $\varepsilon_r = 6.7$), with height H and radius R. The dual-layer metasurface configuration is illustrated in Figures 1(b) and 1(c), showing the upper metasurface layer and lower metasurface layer respectively. Both metasurface layers comprise 16 rectangular unit cells rotated by 45° in a 4×4 array configuration, with the upper-layer cells having width W_1, length L_1, and inter-cell spacing D_1. The lower-layer unit cells feature width W_2 and length L_2, while maintaining the same spacing D_1 between adjacent elements. Both layers use Rogers 5880 dielectric substrates with thickness h, side length L, relative permittivity of 2.2, and loss tangent of 0.0009. The bottom feeding substrate also employs Rogers 5880 material with identical thickness h. The substrate's upper surface serves as the ground plane, featuring an asymmetric X-shaped slot along the X-axis with geometric parameters L_3, L_4, and W_3. A microstrip feed line is symmetrically placed along the X-axis on the substrate's bottom surface, with length L_5 and width W_4. The detailed dimensional parameters are summarized in Table 1.

2.2. Antenna Design Process

Figure 2 clearly illustrates the design evolution of the proposed antenna. Figure 2(a) shows Antenna Model 1 featuring a con-

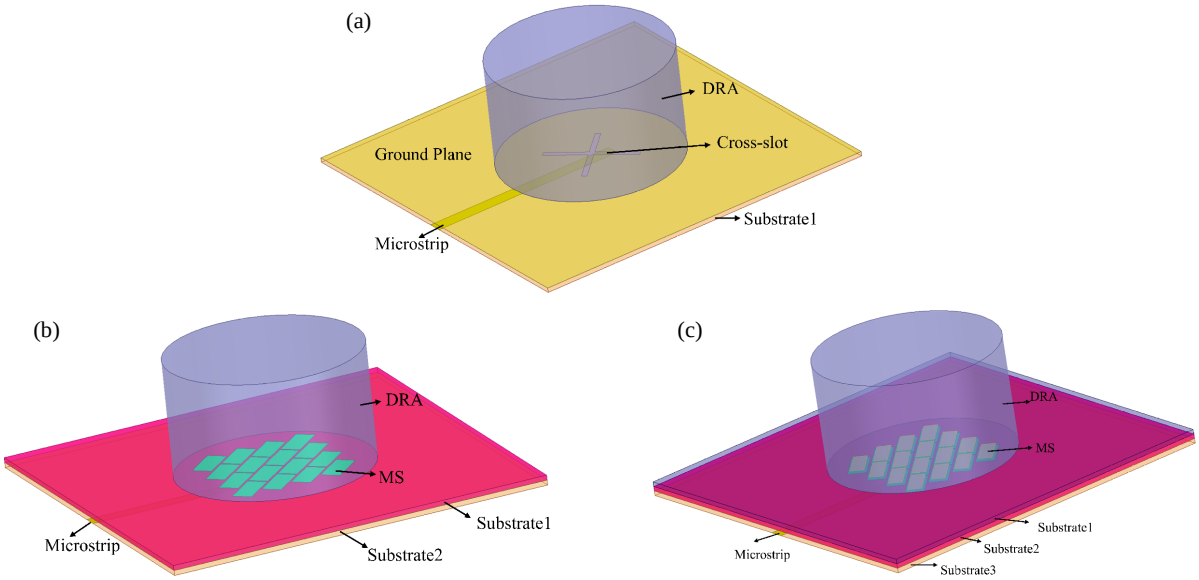

FIGURE 2. The proposed antenna and two reference antennas. (a) Antenna 1. (b) Antenna 2. (c) The proposed antenna.

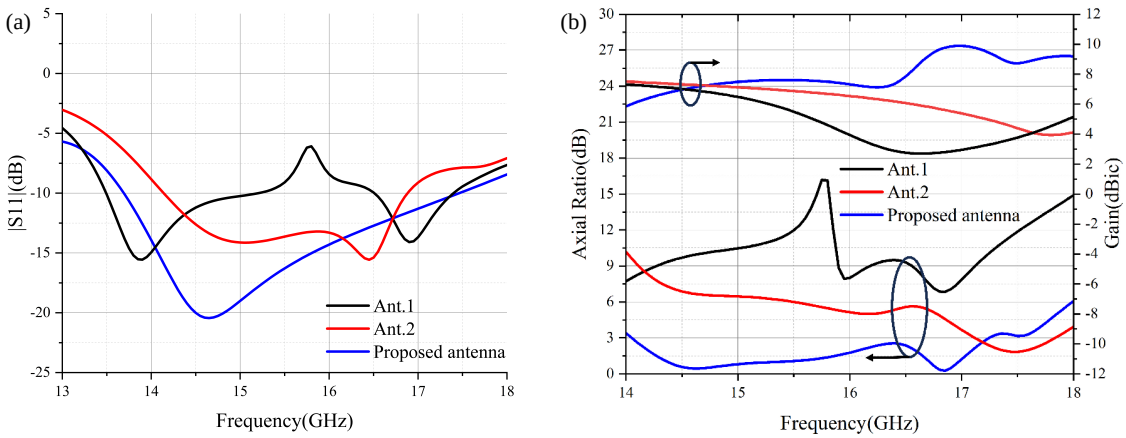

FIGURE 3. Reflection coefficient, axial ratio, and gain of the proposed antenna compared with two reference antennas. (a) Reflection coefficient curves. (b) Axial ratio and gain curves.

TABLE 1. Antenna geometry.

Parameters	L	W_1	L_1	D_1	W_2	L_2	h
Value/mm	20	0.75	1.95	1.58	1	2.14	0.254
Parameters	H	R	L_3	L_4	W_3	L_5	W_4
Value/mm	6	5	5.1	4.5	0.3	11.35	0.76

ventional cylindrical dielectric resonator. Figure 2(b) presents Antenna Model 2, which adds a metasurface layer to the feeding substrate of Model 1. Figure 2(c) displays the proposed antenna, which adds another metasurface layer to Model 2 to form a dual-layer metasurface structure. The dual-layer metasurface acts as a partial reflector. When the inter-layer spacing satisfies resonance conditions, electromagnetic waves undergo multiple reflections within the cavity, with transmitted waves combining in-phase at each reflection, thereby enhancing antenna gain. The metasurface improves circular polarization performance through its electromagnetic wave manipulation capability.

As shown in Figure 3 comparing the performance of the proposed antenna with Antenna 1 and Antenna 2, the introduction of metasurface structures significantly enhances the antenna's performance parameters. Although the single-layer metasurface configuration achieves circular polarization, its axial ratio bandwidth remains relatively narrow. Compared to the single-layer metasurface antenna, the dual-layer version not only broadens the axial ratio bandwidth but also increases the gain.

2.3. Working Principle of the Proposed Antenna

The DRA's resonant frequency may be preliminarily estimated through the Dielectric Waveguide Model (DWM). By modeling the DRA surface as an ideal magnetic conductor, the transverse electric (TE) and transverse magnetic (TM) mode wave func-

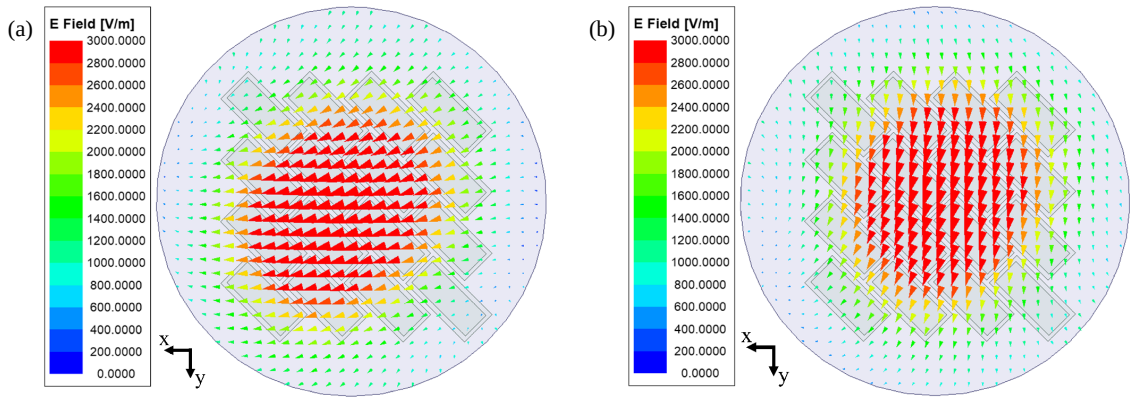

FIGURE 4. Electric field at 16.85 GHz. (a) $\phi = 0°$. (b) $\phi = 90°$.

tions of the DRA can be expressed as [14]:

$$\psi_{TE_{npm}} = J_n\left(\frac{2X_{np}}{D}\rho\right)\begin{pmatrix}\sin(n\phi)\\ \cos(n\phi)\end{pmatrix}\sin\left[\frac{(2m+1)\pi z}{2H}\right] \quad (1)$$

$$\psi_{TM_{npm}} = J'_n\left(\frac{2X'_{np}}{D}\rho\right)\begin{pmatrix}\sin(n\phi)\\ \cos(n\phi)\end{pmatrix}\cos\left[\frac{(2m+1)\pi z}{2H}\right] \quad (2)$$

where J_n is the Bessel function of the first kind, with $J_n(X_{np}) = 0$ and $J'_n(X'_{np}) = 0$, $n = 1, 2, 3, \ldots$, $p = 1, 2, 3, \ldots$, $m = 1, 2, 3, \ldots$.

From the separation equation $k_\rho^2 + k_z^2 = k^2 = \omega^2\mu\varepsilon$, for cylindrical dielectric resonator antennas (DRAs), the resonant frequency of npm modes may be determined by the following equation:

$$f_{npm} = \frac{1}{\pi D\sqrt{\mu\varepsilon}}\sqrt{\begin{pmatrix}X_{np}^2\\ X_{np}'^2\end{pmatrix} + \left[\frac{\pi D}{4H}(2m+1)\right]^2} \quad (3)$$

where $\varepsilon = \varepsilon_0 \times \varepsilon_r$. D is the diameter, and H is the height of the cylindrical dielectric resonator.

Metasurfaces, as two-dimensional equivalents of three-dimensional metamaterials, comprise surface distributions of electrically small scatterers that can control and manipulate electromagnetic waves and radiator emission mechanisms [23]. Metasurfaces can clearly explain how they generate circular polarization performance through the equivalent circuit method, and the impedance formula of the metasurface equivalent circuit is:

$$Z = 2R + j\omega(2L) + \frac{2}{j\omega C} = R + jX \quad (4)$$

As illustrated in Figures 1(b) and 1(c), the electric field of the metasurface can be decomposed into two orthogonal components E_1 and E_2 along the u and v directions, respectively. Due to the structural asymmetry of the metasurface in these directions, the equivalent circuit impedances corresponding to E_1 and E_2 (denoted as Z_1 and Z_2) differ. By adjusting key dimensional parameters of the metasurface, such as W_1 and L_1, the equivalent impedances Z_1 and Z_2 can be independently tuned. When the conditions $|Z_1| = |Z_2|$ and a 90° phase difference are simultaneously satisfied, the metasurface achieves circular polarization performance.

For deeper investigation of the circularly polarized radiation principle, Figure 4 displays the E-field vector patterns at 0° and 90° phase angles corresponding to the 16.85 GHz axial ratio minimum.

The observed field distribution in Figure 4(a) — featuring a diminished x-component while maintaining single-peak/double-node characteristics along all axes — confirms the quasi-TE^x_{111} fundamental mode. Modal analysis of Figure 4(b) confirms a quasi-TE^y_{111} fundamental mode with 90° clockwise rotation of the E-field vector around $+Z$-axis between 0° and 90° phases and maintained amplitude equality. These orthogonal modes generate well-defined left-hand circular polarization (LHCP) radiation.

3. RESULT AND DISCUSSION

The cylindrical dielectric resonator was fabricated via mechanical machining, while the feeding substrate was produced using printed circuit board (PCB) technology. After assembly, the S-parameters were measured using an Agilent Network Analyzer E5071C, and the far-field characteristics of the antenna were evaluated with a Satimo StarLab system to verify its performance. A prototype of the antenna is depicted in Figure 5, where Figure 5(a) shows the top view of the metasurface structure; Figure 5(b) presents the top view of the dielectric resonator antenna (DRA); and Figure 5(c) illustrates the antenna measurement setup.

Figure 6 presents the impedance bandwidth characteristics, where the DRA achieves a -10 dB input impedance bandwidth of 24.2% (13.69–17.46 GHz).

Figure 7 displays the reflection phase curve of the antenna, showing that the frequency range with reflection phase within ±90° is (13.45–17.25 GHz), which is largely consistent with the impedance bandwidth.

Figure 8 presents the axial ratio and gain characteristics of the proposed antenna. As observed in Figure 8, the antenna achieves a 3-dB axial ratio bandwidth of 20.01% (14.05–17.2 GHz). This axial ratio bandwidth is fully functional as it is entirely contained within the impedance bandwidth. Moreover,

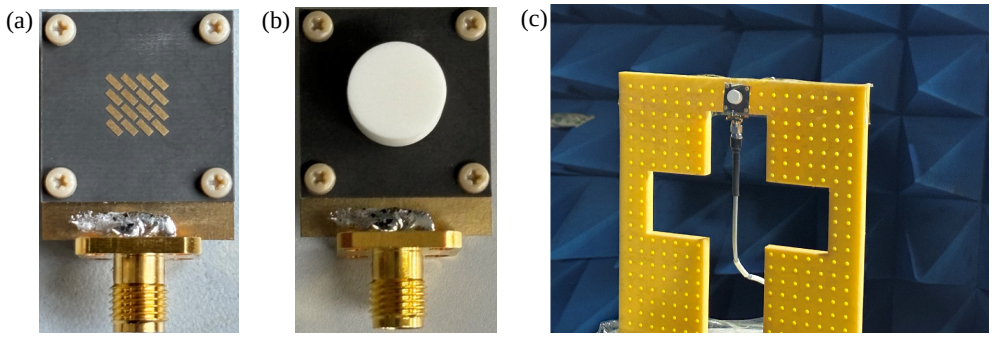

FIGURE 5. Antenna prototype. (a) Metasurface structure. (b) DRA. (c) Antenna measurement diagram.

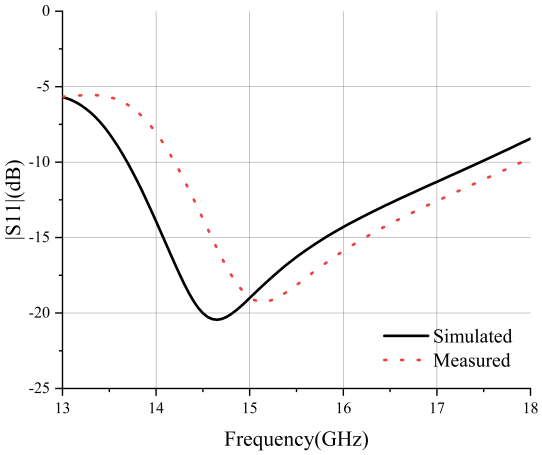

FIGURE 6. Measured and simulated reflection coefficients of the proposed antenna.

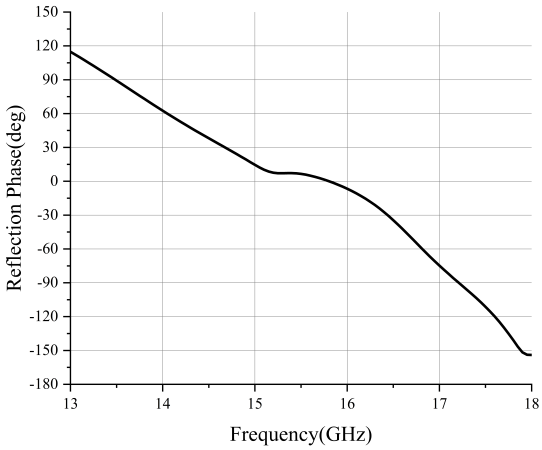

FIGURE 7. Simulated reflection phase of the proposed antenna.

TABLE 2. Comparison with previously reported work in literature.

REF	Impedance BW (%)	Overlapping BW (%)	Gain max (dBi)	Excitation method
[9]	35	22.6	10	Dual-feed
[14]	5.1	1.5	6.03	Single-feed
[17]	15.6	9.8	10.3	Single-feed
[18]	8.26	2.97	15.5	Single-feed
Proposed work	24.2	20.01	9.89	Single-feed

the antenna maintains stable high gain across this bandwidth, reaching a peak gain of 9.89 dBi.

Figure 9 shows the radiation patterns at the minimum axial ratio frequency (16.85 GHz). As expected, broadside radiation patterns are observed in both $\phi = 0°$ and $\phi = 90°$ planes. The LHCP field strength exceeds right-hand circular polarization (RHCP) by more than 20 dBi in both principal planes, confirming excellent LHCP antenna performance.

Table 2 presents a comparative analysis between the proposed antenna and previously reported circularly polarized DRAs. In [9], a sequential tree-shaped array structure is employed. Although this structure demonstrates relatively good performance, it introduces complex power dividing networks (power splitters) and hybrid coupling networks. The complexity of these network structures significantly increases the difficulty of antenna design. Moreover, from the perspective of performance stability, the complex network structures also render the antenna more sensitive to manufacturing errors and environmental changes. In contrast, the antenna proposed in this paper achieves axial ratio bandwidth and gain performance comparable to that in [9] while avoiding the complication of antenna design. Compared with [14], the proposed antenna demonstrates superior bandwidth and gain performance. While achieving similar gain performance to [17], our design exhibits broader impedance and axial ratio bandwidths. Relative to [18], the current work shows improved impedance and axial ratio bandwidths though with slightly lower gain. In summary, the proposed antenna achieves an optimal balance among impedance bandwidth, axial ratio bandwidth, and gain, showing excellent potential for KU-band applications.

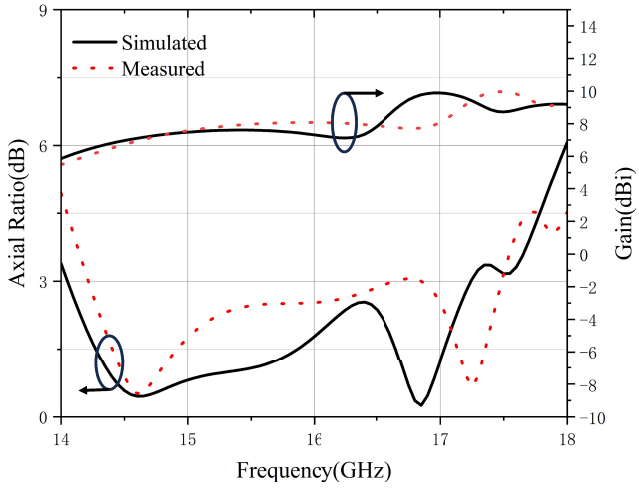

FIGURE 8. Measured and simulated axial ratio and gain of the proposed antenna.

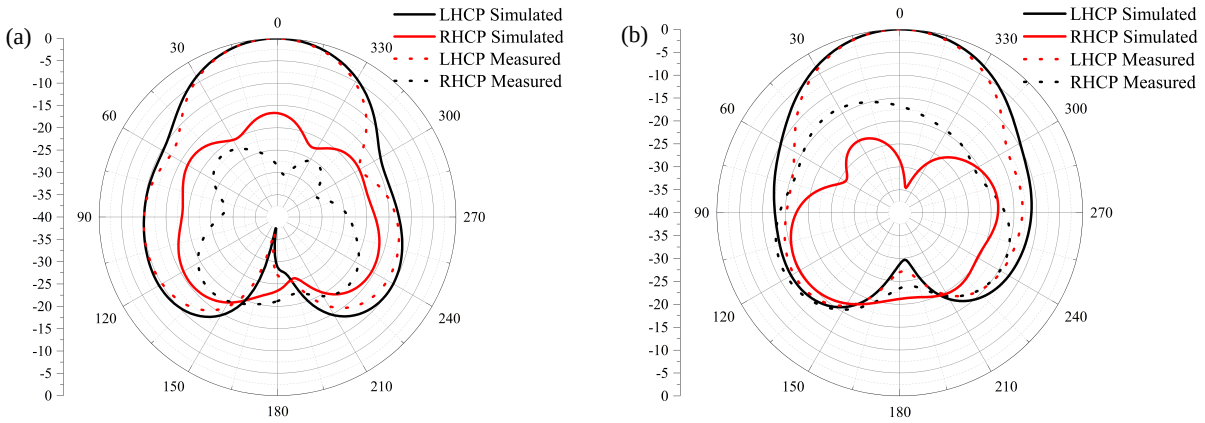

FIGURE 9. Radiation patterns of proposed antenna at 16.85 GHz. (a) $\phi = 0^\circ$. (b) $\phi = 90^\circ$.

4. CONCLUSION

This paper presents the design of a broadband circularly polarized dielectric resonator antenna (DRA) loaded with a double-layer metasurface structure. By employing asymmetric X-shaped slot coupling for feeding to generate orthogonal modes and leveraging the polarization manipulation characteristics of the double-layer metasurface structure, the axial ratio bandwidth of the DRA is significantly broadened, and the gain is enhanced. The proposed antenna offers advantages such as broadband operation, circular polarization, high gain, and a simple feeding structure. It operates in the KU-band, showing promising applications in wireless communications including satellite communication and global satellite positioning systems.

ACKNOWLEDGEMENT

This work is supported by Tianjin Key Projects of Research and Development and Science and Technology Support in 2020 (20YFZCGX00700), Tianjin Enterprise Science and Technology Commissioner Project in 2022 (22YDTPJC00330) and 2024 Tianjin Natural Science Foundation (24JCYBJC00860).

REFERENCES

[1] Long, S., M. McAllister, and L. Shen, "The resonant cylindrical dielectric cavity antenna," *IEEE Transactions on Antennas and Propagation*, Vol. 31, No. 3, 406–412, May 1983.

[2] Mongia, R. K. and P. Bhartia, "Dielectric resonator antennas — A review and general design relations for resonant frequency and bandwidth," *International Journal of Microwave and Millimeter-Wave Computer-Aided Engineering*, Vol. 4, No. 3, 230–247, Jul. 1994.

[3] Petosa, A. and A. Ittipiboon, "Dielectric resonator antennas: A historical review and the current state of the art," *IEEE Antennas and Propagation Magazine*, Vol. 52, No. 5, 91–116, Oct. 2010.

[4] Ren, J., Z. Wang, Y.-X. Sun, R. Huang, and Y. Yin, "Ku/Ka-band dual-frequency shared-aperture antenna array with high isolation using frequency selective surface," *IEEE Antennas and Wireless Propagation Letters*, Vol. 22, No. 7, 1736–1740, Jul. 2023.

[5] Ding, Y. R., Y. J. Cheng, J. X. Sun, L. Wang, and T. J. Li, "Dual-band shared-aperture two-dimensional phased array antenna with wide bandwidth of 25.0% and 11.4% at Ku-and Ka-band," *IEEE Transactions on Antennas and Propagation*, Vol. 70, No. 9, 7468–7477, Sep. 2022.

[6] Mongia, R. K. and P. Bhartia, "Dielectric resonator antennas — A review and general design relations for resonant fre-

quency and bandwidth," *International Journal of Microwave and Millimeter-Wave Computer-Aided Engineering*, Vol. 4, No. 3, 230–247, Jul. 1994.

[7] Toh, B. Y., R. Cahill, and V. F. Fusco, "Understanding and measuring circular polarization," *IEEE Transactions on Education*, Vol. 46, No. 3, 313–318, Aug. 2003.

[8] Petosa, A., *Dielectric Resonator Antenna Handbook*, Artech House, 2007.

[9] Attia, H., A. Abdalrazik, M. S. Sharawi, and A. A. Kishk, "Wideband circularly polarized millimeter-wave DRA array for internet of things," *IEEE Internet of Things Journal*, Vol. 10, No. 11, 9597–9606, Jun. 2023.

[10] Liu, W.-W., Z.-H. Cao, and Z. Wang, "A wideband circularly polarized dielectric resonator antenna array," *IEEE Access*, Vol. 9, 99 589–99 594, Jul. 2020.

[11] Dash, U. A., D. Dutta, and S. Pahadsingh, "Circularly polarized stepped rectangular DRA for mid-band 5G application," in *2023 IEEE 3rd International Conference on Applied Electromagnetics, Signal Processing, & Communication (AESPC)*, 1–4, Bhubaneswar, India, Nov. 2023.

[12] Kumar, R., D. K. Choudhary, R. Singh, and R. K. Chaudhary, "A wideband circularly polarized DRA excited with meandered-line inductor for Wi-MAX/LTE2500 applications," in *2017 Progress in Electromagnetics Research Symposium — Fall (PIERS — FALL)*, 1514–1519, Singapore, Nov. 2017.

[13] Varshney, G., "Gain and bandwidth enhancement of a singly-fed circularly polarised dielectric resonator antenna," *IET Microwaves, Antennas & Propagation*, Vol. 14, No. 12, 1323–1330, Oct. 2020.

[14] Zhao, G., Y. Zhou, J. R. Wang, and M. S. Tong, "A circularly polarized dielectric resonator antenna based on quasi-self-complementary metasurface," *IEEE Transactions on Antennas and Propagation*, Vol. 70, No. 8, 7147–7151, 2022.

[15] Elahi, M., A. Altaf, Y. Yang, K.-Y. Lee, and K. C. Hwang, "Circularly polarized dielectric resonator antenna with two annular vias," *IEEE Access*, Vol. 9, 41 123–41 128, Mar. 2021.

[16] Tong, C., H. I. Kremer, N. Yang, and K. W. Leung, "Compact wideband circularly polarized dielectric resonator antenna with dielectric vias," *IEEE Antennas and Wireless Propagation Letters*, Vol. 21, No. 6, 1100–1104, 2022.

[17] Perron, A., T. A. Denidni, and A. R. Sebak, "Circularly polarized microstrip/elliptical dielectric ring resonator antenna for millimeter-wave applications," *IEEE Antennas and Wireless Propagation Letters*, Vol. 9, 783–786, 2010.

[18] Akbari, M., S. Gupta, M. Farahani, A. R. Sebak, and T. A. Denidni, "Gain enhancement of circularly polarized dielectric resonator antenna based on FSS superstrate for MMW applications," *IEEE Transactions on Antennas and Propagation*, Vol. 64, No. 12, 5542–5546, Dec. 2016.

[19] Faenzi, M., G. Minatti, D. González-Ovejero, F. Caminita, E. Martini, C. D. Giovampaola, and S. Maci, "Metasurface antennas: New models, applications and realizations," *Scientific Reports*, Vol. 9, No. 1, 10178, Jul. 2019.

[20] Bukhari, S. S., J. Vardaxoglou, and W. Whittow, "A metasurfaces review: Definitions and applications," *Applied Sciences*, Vol. 9, No. 13, 2727, Jul. 2019.

[21] Nasimuddin, N., Z. N. Chen, and X. Qing, "Bandwidth enhancement of a single-feed circularly polarized antenna using a metasurface: Metamaterial-based wideband cp rectangular microstrip antenna," *IEEE Antennas and Propagation Magazine*, Vol. 58, No. 2, 39–46, 2016.

[22] Sheersha, J. A., N. Nasimuddin, and A. Alphones, "A high gain wideband circularly polarized antenna with asymmetric metasurface," *International Journal of RF and Microwave Computer-Aided Engineering*, Vol. 29, No. 7, e21740, 2019.

[23] Park, I., "Application of metasurfaces in the design of performance-enhanced low-profile antennas," *EPJ Applied Metamaterials*, Vol. 5, 11, 2018.